JOURNAL OF NANO- AND ELECTRONIC PHYSICS
Vol. **11** No 2, 02012(5pp) (2019)

ЖУРНАЛ НАНО- ТА ЕЛЕКТРОННОЇ ФІЗИКИ
Том **11** № 2, 02012(5cc) (2019)

Optical Properties of *in-situ* Chemically Synthesized PANI-TiO_2 Nanocomposites

Ajay Kumar Sharma[1,2,*], Rishi Vyas[2], Praveen Kumar Jain[3], Umesh Chand[4], Vipin Kumar Jain[1]

[1] *Institute of Engineering and Technology, JK Lakshmipat University, Jaipur 302026, India*
[2] *Department of Physics, Swami Keshvanand Institute of Technology, Management & Gramothan, Jaipur 302017, India*
[3] *Department of Electronics and Communication Engineering, Swami Keshvanand Institute of Technology, Management & Gramothan, Jaipur 302017, India*
[4] *Department of Electrical and Computer Engineering, National University of Singapore, Singapore*

(Received 07 December 2018; revised manuscript received 03 April 2019; published online 15 April 2019)

The present manuscript details on the synthesis of $(PANI)_{1-x}(TiO_2)_x$ nanocomposite ($x = 0$, 0.02, 0.04, 0.06, 0.08, 0.10) using an in-situ chemical oxidation polymerization of aniline using ammonium peroxide sulfate (APS) as an oxidant in presence of colloidal anatase TiO_2 nanoparticles at 0-5 °C in air. The X-ray diffraction of these specimens revealed amorphous nature of polyaniline which did not change with the addition of TiO_2 nanoparticles during polymerization process. The selected area electron diffraction (SAED) pattern obtained from TEM also indicated the amorphous nature of polyaniline. The TiO_2 nanoparticles exhibit diffraction from multiple lattice planes originating from polycrystalline nature of nanoparticles. The SAED pattern corresponding to the nanocomposite displays lattice planes showing inter planar spacing of 3.56 Å resulting from (101) lattice planes of TiO_2 nanoparticles. To study the vibration mode of PANI and PANI-TiO_2 nanocomposites, Raman spectra was observed. Absorption spectra of the nanocomposite samples have been taken using UV-VIS-NIR spectrophotometer (Varian Cary 5000). The band gap energy (E_g) of the nanocomposites was determined using Talc's relationship. As the content of TiO_2 was increased in the polymer matrix, the shift of the optical band gap was observed.

Keywords: X-ray spectra, UV-Vis spectra, Structure of nanoscale materials, Dielectric properties of solids and liquids.

DOI: 10.21272/jnep.11(2).02012

PACS numbers: 32.30.Rj, 33.20.Lg, 61.46. – W, 77.22. – d

1. INTRODUCTION

The nanocomposites have been explored at great lengths in recent past due to their unique properties which were not available in their constituent materials. Conducting polymers are one such class of materials which exhibit unique electrical, optical and chemical properties, but their usage is limited due to their limited thermal stability. These conducting polymers find application in information storage, optical signal processing, batteries, and solar energy conversion [1-2]. Polyaniline (PANI) is one such conducting polymer, which is a candid photosensitizer due to its low band gap, π-*π transition in which the electron can be excited from the highest occupied molecular orbital (HOMO) to the lowest unoccupied molecular orbital (LUMO), high conductivity, good environmental stability, cheap monomer, and ease of preparation [3-5]. In line with other conducting polymers, PANI also suffers from lesser thermal stability which limits its applications. The synthesis of a composite material of PANI with any other component exhibiting superior thermal stability could present a new material with better characteristics for optoelectronic applications [6].

TiO_2 is one such material exhibiting excellent photocatalytic properties along with higher chemical stability, nontoxic and relatively low-price. Titanium (IV) oxide is found in rutile, anatase, brooked three polymorphic forms [7]. Among these forms, rutile and anatase phases are quite popular as a base for the use as pigments, catalysts and in the production of ceramic and electronic materials. On the other hand, the bottlenecks for TiO_2 usages such as wide band gap (3.2 eV) and low electrical conductance (1.1×10^{-5}-3.4×10^{-3} Ω/cm) could easily be addressed by mixing it with PANI [8-11]. The anatase TiO_2 is selected in this study which is more efficient as a photocatalyst than rutile form. Further, the clusters of TiO_2 formed during the composite formation can absorb UV energy which makes them suitable for photocatalytic application. The PANI in composite material can be decomposed by oxidation due to the presence of radicals released by irradiation and thus are useful as photocatalyst. Therefore, the contribution of higher conductivity from PANI and higher thermal stability of TiO_2 could complement each other in making new composite material with superior properties [12-14].

2. EXPERIMENTAL DETAILS

In-situ chemical oxidative polymerization method at lower temperature between 0-5 °C was used for synthesis of PANI, which has been reported earlier [15-16]. The $(PANI)_{1-x}(TiO_2)_x$ nanocomposite ($x = 0$, 0.02, 0.04, 0.08, 0.10) was prepared by an in-situ chemical oxidation polymerization of aniline using ammonium peroxide sulfate (APS) as an oxidant in the presence of an appropriate amount of colloidal TiO_2 nanoparticles at 0-5 °C in air. The obtained powder is washed multiple times and dried in vacuum before the structural, optical and dielectric measurements. The crystallinity of PANI, TiO_2 and PANI-TiO_2 nanocomposites is estimated by X-ray diffractometry (XRD, Bruker AXS D-8

* ajaymnit19@gmail.com

Advance Diffractometer) using Cu-Kα ($\lambda = 1.5407$ Å) radiation and selected area electron diffraction (SAED) pattern obtained from TEM (Tecnai G 2 20 (FEI) S-Twin). The surface topology of specimens was investigated by Scanning Electron Microscopy (SEM) on quanta FESEM 450 (FEI). Raman spectra of PANI-TiO_2 nanocomposites were measured using confocal Raman microscopy. Absorption spectra of the nanocomposites were observed using UV-Vis-NIR spectrophotometer (LAMBDA 750, Perkin Elmer).

3. RESULTS AND DISCUSSION

3.1 Structural Characterization

The X-ray diffraction patterns corresponding to PANI and PANI-TiO_2 nanocomposites are plotted in Fig. 1 which are indicative of an amorphous hump with no evidence of crystallinity corresponding to PANI, while a sharp peak at 25.19° is observed for PANI-TiO_2 nanocomposites, which is due to diffraction from (101) lattice planes of anatase phase of TiO_2. Furthermore, the peak intensity of diffraction from (101) lattice planes of TiO_2 was increasing with the concentration of TiO_2 in the nanocomposite.

The crystallite size of PANI-TiO_2 nanocomposite crystallites was estimated as ~ 37 nm, which is fairly equal to the particle size of TiO_2 nanoparticles used for making nanocomposites indicating no crystal growth during synthesis of nanocomposites.

The size of PANI-TiO_2 nanocomposite crystallites was estimated correspond to prominent peak indexed (101-A) having a FWHM of 0.215° using the Debye-Scherrer's equation [17]:

$$t = \frac{0.94\lambda}{\beta \cos\theta}, \qquad (3.1)$$

where β is the FWHM (full width at half maxima of diffraction peak in radians), t is the grain size, λ is the X-ray wavelength (Cu-Kα is used in the present study), cos θ is the cosine of the Bragg angle θ. The estimated grain size of PANI-TiO_2 nanocomposite was 40.88 nm.

The image of pure PANI recorded with transmission electron microscopy (TEM) is shown in Fig. 2b, which implies a uniform structure with some dark regions originating from the denser regions of PANI. The SAED pattern corresponding to PANI is shown in Fig. 2a, which is indicative of amorphous nature of the PANI specimen. It enunciates the results obtained from X-ray diffraction study.

Fig. 2c, d shows the TEM images of PANI-TiO_2 (10 %) nanocomposite which is indicative of cluster formation of various sizes and shapes. A hazy layer around these clusters is indicative of TiO_2 clusters embedded in PANI. The HRTEM image of PANI-TiO_2 (10 %) nanocomposite is shown in Fig. 2d, which shows the crystalline planes with interplanar distance of 0.356 nm. This interlayer spacing corresponds to the plane (101-A) in X-ray diffraction spectra according to the formulation of Bragg's law.

The surface topology of PANI and its nanocomposites is shown in Fig. 3. Fig. 3a displays the relatively flat layered structure of pure PANI, while Figs. 3b-f indicate the agglomerated grains in PANI.

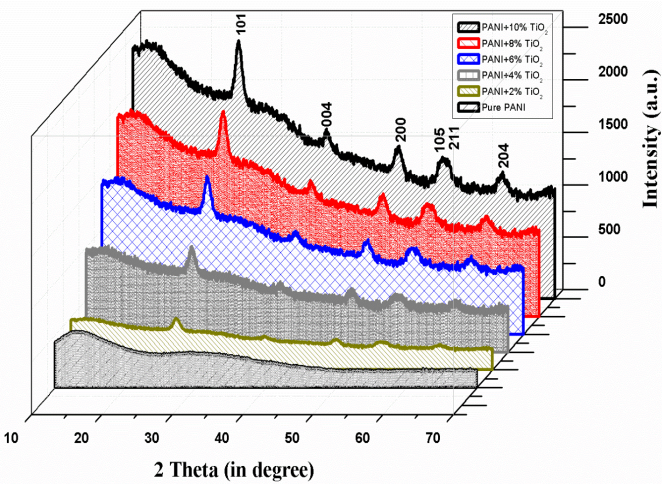

Fig 1 – X-ray diffraction patterns of pure PANI and PANI-TiO_2 nanocomposites

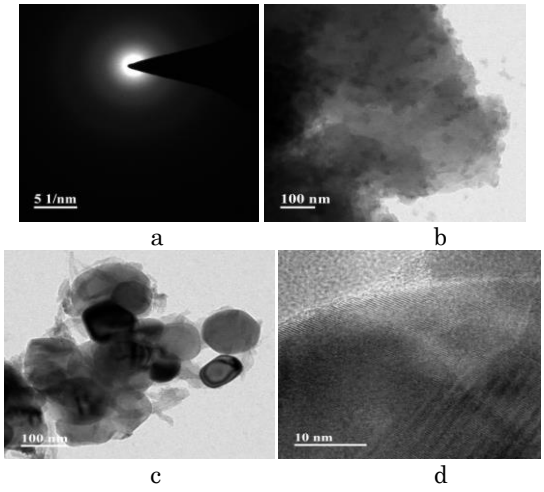

Fig. 2 – SAED image of (a) pure PANI, TEM images of (b) pure PANI and (c, d) PANI-TiO_2 (10 %) nanocomposites

The polymerization of aniline has taken place on the surface of TiO_2 nanoparticles which has resulted in the visible lumps with TiO_2 at its core. Further, the presence of similar lumps on the surface indicates uniform distribution of TiO_2 in nanocomposites.

The Raman spectra of PANI and PANI-TiO_2 nanocomposites are taken to obtain knowledge about the change in the fundamental vibration mode of PANI-TiO_2 on formation of nanocomposites. The Raman spectra are shown in Fig. 4 which is indicative of lesser intensity peak corresponding to pure PANI. It indicates the less scattering of laser originated from few crystalline planes of PANI. PANI exhibited peaks of smaller intensity near 406, 509, 575 (shown by blue arrow in Fig. 4), 825, 1183, 1249, 1341, 1507, and 1603 cm^{-1} (not shown here). Among these peaks, peaks centering at 1603 and 509 cm^{-1} correspond to the C=C stretching vibrations of benzenoid and quinoid rings, respectively, while the signature of C-H bending vibration of benzene quinoid ring is observed in the form of peaks at 1341 and 1183 cm^{-1}, respectively [18]. The Raman spectra of nanocomposites yield higher intensity peaks at 144 cm^{-1}, 397 cm^{-1}, 520 cm^{-1}, and 640 cm^{-1}, which are indicative of the presence of lattice vibration

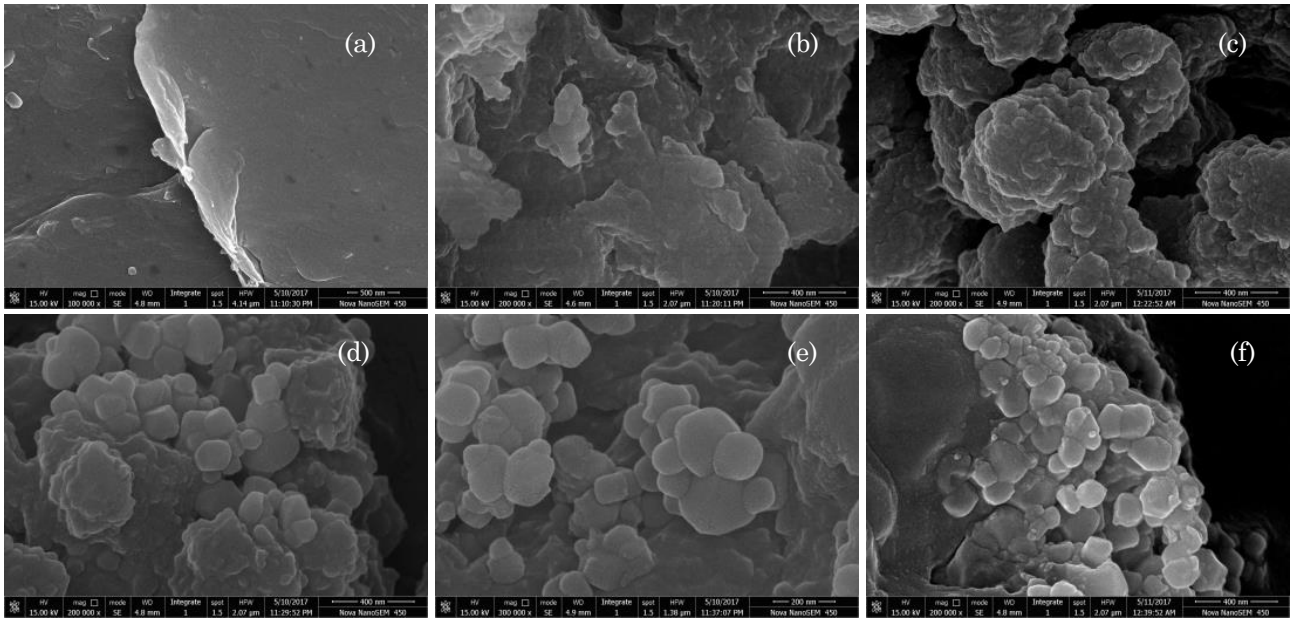

Fig. 3 – SEM images of (a) pure PANI, (b) PANI-TiO_2 (2 %), (c) PANI-TiO_2 (4 %), (d) PANI-TiO_2 (6 %), (e) PANI-TiO_2 (8 %) and (f) PANI-TiO_2 (10 %)

corresponding to the vibration modes E_g, B_{1g}, A_{1g}/B_{1g} and E_g, respectively, of TiO_2 lattice [19]. The Raman results conclude no change in the Raman shift corresponding to the nanocomposites which indicate stability of individual structure of PANI and TiO_2 in nanocomposites afterwards the formation of nanocomposites.

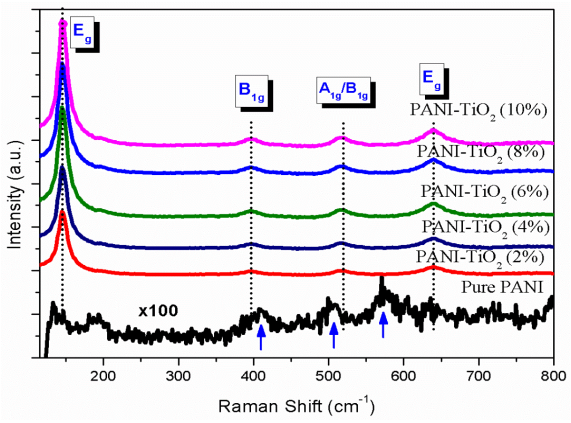

Fig. 4 – Raman spectra of pure PANI and PANI-TiO_2 nanocomposites

3.2 Optical Properties

Fig. 5a shows the UV-Vis absorption spectra of pure PANI and PANI-TiO_2 nanocomposites. The absorption curve can be broken down in four regions: (i) 180 nm-220 nm, (ii) 220 nm-250 nm, (iii) 250 nm-300 nm, (iv) beyond 300 nm. No change was observed in the shape of the spectra in the spectral regions (ii), (iii) and (iv) other than the variation in intensity with addition of TiO_2 in PANI which is due to good absorption property of TiO_2 nanoparticles. However, a small shift in the band edge in the regions (i) and (iii) was observed. It may be due to the encapsulation of TiO_2 nanoparticles in conducting PANI and formation of coordinate complex between TiO_2 nanoparticles and PANI chains [20-21].

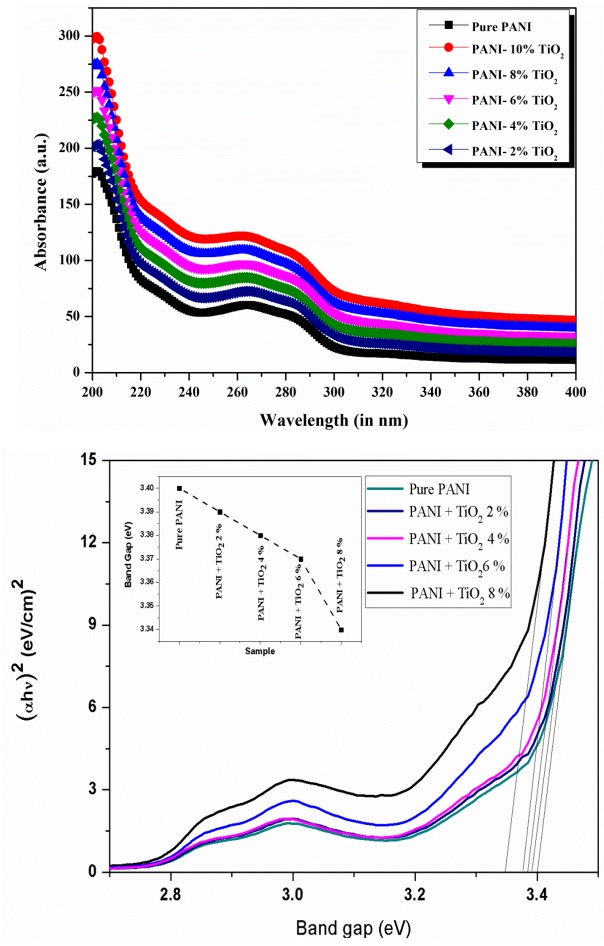

Fig. 5 – (a) UV-Vis absorption spectrum for PANI and PANI-TiO_2 nanocomposites and (b) $(\alpha h\nu)^2$ vs hν plot for PANI and PANI-TiO_2 nanocomposites

The optical band gap is obtained according to Tauc's model from UV-Vis spectra using the relation [22]

$$\alpha h\upsilon = A\left(h\upsilon - E_g\right)^n \qquad (3.2)$$

where α is the absorption coefficient, h is the Planck's constant, υ is the frequency of light, E_g is the band gap, 'n' is 2 for an indirect transition or 1/2 for a direct transition and A is a constant.

A Tauc's plot is shown in Fig 5b displaying the band gap determination for PANI and PANI-TiO_2 nanocomposites. The band gap of PANI is observed at 3.40 eV which is similar to the other reports [23]. A decrease in the band gap with the addition of TiO_2 is also observed from 3.40 eV to 3.34 eV with 8 % TiO_2 which is favorable considering the lower band gap of TiO_2. The change in the band gap is indicative of modified absorbance of coordinate complex formed between TiO_2 and PANI chains, which are exhibiting a decreasing trend due to increased concentration of TiO_2 nanoparticles in nanocomposites [24, 25].

4. CONCLUSIONS

PANI and PANI-TiO_2 nanocomposites were successfully fabricated. XRD spectra exhibit diffraction peaks corresponding to various planes of TiO_2, while pure PANI exhibits amorphous nature. The SEM images helped to conclude that the doping of TiO_2 had a strong effect on PANI morphology. It is shown that the dispersion of TiO_2 nanocrystals influences the morphology of PANI greatly. The SEM micrograph of PANI-TiO_2 is not so much smooth and so many uneven lumps are clearly visible. Raman spectra confirm the formation of PANI-TiO_2 nanocomposites. The absorbance in the UV-Vis spectra is observed to increase in the whole range of UV-Vis wavelength with the increase in the concentration of TiO_2 in PANI-TiO_2 nanocomposites. The corresponding Tauc's plots show the shift in the band gap from 3.40 eV to 3.34 eV with an increase in the concentration of TiO_2 in the nancomposites.

REFERENCES

1. A. Moliton, R.C. Hiorns, *Polymer Int.* **53**, 1397 (2004).
2. H. Banno, K. Ogura, *Ferroelectrics* **95**, 111 (1989).
3. V. Eskizeybek, F. Sari, H. Gulce, A. Gulce, A. Avci, *Appl. Catalysis B: Environmen.* **119**, 197 (2012).
4. M.M. Kerileng, M.N. Peter, F.A. Rachel, M. Gcineka, M.M. Stephen, N. Njagi, M. Milua, B. Priscilla, *Int. J. Electrochem. Sci.* **7**, 11859 (2012).
5. S.P. Ansari, F. Mohammad, *Polymer. Polymer Compos.* **24(4)**, 273 (2016).
6. Q.L. Hao, X.F. Xia, W. Lei, W.J. Wang, J.S. Qiu, *Carbon* **81**, 552 (2015).
7. J. Tang, F. Redl, Y. Zhu, T. Siegrist, L.E. Brus, M.L. Steigerwald, *Nano Lett.* **5(3)**, 543 (2005).
8. S.C. Raghavendra, S. Khasim, M. Revanasiddappa, M.V.N.A. Prasadand, A.B. Kulkarni, *Bull. Mater. Sci.* **26(7)**, 733 (2003).
9. M.D. Butterworth, R. Corradi, J. Johal, S.F. Lascelles, S. Maeda, S.P. Armes, *J. Colloid Interface Sci.* **174(2)**, 510 (1995).
10. A. Dan, P.K. Sengupta, *J. Appl. Polymer Sci.* **91(2)**, 991 (2003).
11. X. Jiang, T. Herricks, Y. Xia, *Adv. Mater.* **15(14)**, 1205 (2003).
12. J.R. Bolton, *Sol. Energ. Mater. Sol. C.* **38**, 543 (1995).
13. A. Harriman, I.J. Pickering, J.M. Thomas, P.A. Christensen, *J. Chem. Soc., Faraday Transact. 1: Physical Chemistry in Condensed Phases* **84(8)**, 2795 (1988).
14. M. Irfan, A. Shakoor, B. Ali, A. Elahi, M.I. Ghouri, A. Ali, *Eur. Academic Res.* **Vol. II (8)**, 10602 (2014).
15. S. Srivastava, S.S. Sharma, S. Kumar, S. Agrawal, M. Singh, Y.K. Vijay, *Int. J. Hydrogen Energy* **34(19)**, 8444 (2009).
16. S. Srivastava, S.S. Sharma, S. Kumar, S. Agrawal, M. Singh, Y.K. Vijay, *Synthetic Metals* **160(5-6)**, 529 (2010).
17. S.M. Reda, S.M. Al-Ghannam, *Adv. Mater. Phys. Chem.* **2**, 75 (2012).
18. M. Trchová, Z. Morávková, M. Bláha, J. Stejskal, *Electrochimica Acta* **122**, 28 (2014).
19. F. Zhang, H. Cao, D. Yue, J. Zhang, M. Qu, *Inorg. Chem.* **51(17)**, 9544 (2012).
20. X. Ma, M. Wang, G. Li, H. Chen, R. Bai, *Mater. Chem. Phys.* **98**, 241 (2006).
21. R. Sainz, W.R. Small, N.A. Young, C. Valles, A.M. Benito, W.K. Maser, *Macromolecules* **39**, 7324 (2006).
22. K.T. Vadiraj, S.L. Belagali, *IOSR J. Appl. Chem.* **8(1)**, 53 (2015).
23. M. Mitra, C. Kulsi, K. Chatterjee, K. Kargupta, S. Ganguly, D. Banerjee, S. Goswamid, *RSC Adv.* **5**, 31039 (2015).
24. R. Cruz-Silva, J. Romero-Garcia, J.L. Angulo-Sanchez, E. Flores-Loyola E, M.H. Farias, F.F. Castillon, *Polymer* **45**, 4711 (2004).
25. X. Li, G. Wang, D. Lu, *Appl. Surf. Sci.* **229**, 395 (2004).

Оптичні властивості хімічно синтезованих нанокомпозитів PANI-TiO_2

Ajay Kumar Sharma[1,2], Rishi Vyas[2], Praveen Kumar Jain[3], Umesh Chand[4], Vipin Kumar Jain[1]

[1] *Institute of Engineering and Technology, JK Lakshmipat University, Jaipur 302026, India*
[2] *Department of Physics, Swami Keshvanand Institute of Technology, Management & Gramothan, Jaipur 302017, India*
[3] *Department of Electronics and Communication Engineering, Swami Keshvanand Institute of Technology, Management & Gramothan, Jaipur 302017, India*
[4] *Department of Electrical and Computer Engineering, National University of Singapore, Singapore*

У роботі представлені результати синтезу нанокомпозиту $(PANI)_{1-x}(TiO_2)_x$ ($x = 0$, 0.02, 0.04, 0.06, 0.08, 0.10) з використанням хімічної окислювальної полімеризації аніліну in-situ з використанням сульфату пероксиду амонію як окислювача у присутності наночастинок колоїдного анатазу TiO_2 при 0-5 °C на повітрі. Рентгенівська дифракція цих зразків виявила аморфну природу поліаніліну, яка не змінювалася при додаванні наночастинок TiO_2 під час процесу полімеризації. Електронограми, отримані з ТЕМ, також показали аморфну природу поліаніліну. Наночастинки TiO_2 демонструють дифракцію від множинних площин ґраток, що походять з полікристалічної природи наночастинок. Електронограма, що відповідає нанокомпозиту, ілюструє площини гратки із міжплощинною відстанню

3.56 Å, отриману з (101) площин ґратки наночастинок TiO_2. Для вивчення вібраційного режиму нанокомпозитів PANI і PANI-TiO_2 спостерігалися спектри комбінаційного розсіювання. Спектри поглинання нанокомпозитних зразків були отримані з використанням спектрофотометра UV-VIS-NIR (Varian Cary 5000). Енергію забороненої зони нанокомпозитів визначали за допомогою співвідношення Талька. При збільшенні вмісту TiO_2 у полімерній матриці спостерігався зсув забороненої зони.

Ключові слова: Рентгенівські спектри, Ультрафіолетові та видимі спектри, Структура нанорозмірних матеріалів, Діелектричні властивості твердих тіл і рідин.